Understanding the enhancement and temperature-dependency of the self-healing and electromechanical properties of dielectric elastomers containing mixed pendant polar groups

Christopher Ellingford,[1] Alan M. Wemyss,[1] Runan Zhang,[2] Ivan Prokes,[3] Tom Pickford,[1] Chris Bowen,[2] Vincent A Coveney, [2] Chaoying Wan[1,*]

[1] *International Institute for Nanocomposites Manufacturing (IINM), WMG, University of Warwick, CV4 7AL, UK*

[2] *Department of Mechanical Engineering, University of Bath, BA2 7AY, UK*

[3] *Department of Chemistry, University of Warwick, CV4 7AL, UK*

Christopher Ellingford, Dr. Alan M. Wemyss, Tom Pickford, Dr Chaoying Wan*
International Institute for Nanocomposites Manufacturing (IINM), WMG, University of Warwick, CV4 7AL, UK
Email: Chaoying.wan@warwick.ac.uk
Dr Runan Zhang, Dr Vincent Coveney, Prof Chris Bowen
Department of Mechanical Engineering, University of Bath, BA2 2ET, UK
Dr Ivan Prokes
Department of Chemistry, University of Warwick, CV4 7AL, UK

Email: Chaoying Wan, chaoying.wan@warwick.ac.uk

Keywords: self-healing, dielectric elastomer, grafted dipoles, temperature-dependent behaviour, intrinsic modification

Abstract

High permittivity self-healing dielectric elastomers have the potential to achieve long life, reusability, damage tolerance and enhanced energy density for energy harvesting devices and actuators. The self-healing performance of elastomers and usable temperature range can be affected by the chemical interactions present in the material. Self-healing thermoplastic elastomer styrene-butadiene-styrene (SBS) copolymers were prepared by introducing hydrogen bonding and electrostatic interactions through chemically grafting of polar groups to

SBS: methyl thioglycolate (MG) and thioglycolic acid (TG). The mechanical properties were significantly affected by the strength of the hydrogen bonding network in the elastomers, whilst a high relative permittivity of $\varepsilon_r \approx 9.2$ with a low loss of $\tan \delta \approx 0.01$ was achieved. In addition, a disorder-to-order phase morphology transition was observed upon increasing the TG content due to the increased hydrogen-bonding network within SBS. At room temperature the self-healed 80/20 MG/TG-SBS exhibited a strain at break of 139% with a recovery ratio of 47.7%, and when healed at 80 °C for 3 hrs exhibited an increased strain at break of 230% with a recovery ratio of 79%. Analysis of FTIR and ^{1}H NMR indicated that the presence of a stronger hydrogen bonding network increased the thermal resistance of the elastomers. The temperature-dependency of the self-healing behaviour was interpreted as the combined effect of hydrogen bonding, electrostatic interactions and chain interdiffusion. This work provides an in-depth understanding of how to tune the electromechanical and self-healing properties of elastomers by tailoring the type and concentration of pendent polar groups. It indicates that intrinsic modification is critical for the development of next generation high performance dielectric elastomers for actuator or energy harvesting devices operating at elevated temperatures.

Introduction

Research to develop new self-healing polymers continues to attract attention since the initial theory of Wool & O'Connor[1, 2] for the different stages of self-healing of a lightly crosslinked hydroxyl-terminated polybutadiene. To create self-healing polymers, an enhancement of the macromolecular interactions can be designed by the incorporation of polar functional groups to the polymer backbone, or grafting as pendant groups. The pendant groups can be introduced through either covalently grafting or forming dynamic covalent bonds between polymer chains.

A variety of chemical reactions have been investigated for the intrinsic modification of polymers to tailor the mechanical, electrical or self-healing behaviour. Whilst thiol-ene click chemistry is typically used for unsaturated polyolefin based polymers, silicone based elastomers utilise hydrosilylation chemistry for modification. Using reversible Diels-Alder chemistry between furfuryl groups and maleimide groups[3], a thermal equilibrium allows covalent interactions to be formed between the two groups and thereby introduces crosslinking of the polymer chains at temperatures of ~80 °C. However, subjecting the material to temperatures above 120 °C results in breakage of the covalent bonds and the presence of

dynamic covalent bonds yield a strong, crosslinked but processable polymer. The dynamic nature of the bonding can also act as a self-healing mechanism for the polymer to adhere two broken sections together[4]. Bai et al. grafted furfuryl mercaptan to styrene-butadiene-styrene (SBS) copolymer which exhibited an ability to self-heal and could be remoulded multiple times[5]. However, there is little tunability with regard to temperature ranges for self-healing using Diels-Alder chemistry, and thus outside of these narrow temperature conditions it is difficult to use successfully.

Interactions between aromatic groups *via* π-π stacking have also been utilised to introduce, or enhance, self-healing into polymers[6]. For example, a supramolecular elastomer derived from sebacic acid and citric acid was grafted with tetraaniline to produce self-healing from both π-π stacking between the aniline groups and hydrogen bonding from functional groups present in the polymer backbone. This resulted in a healing efficiency of 92.5% with regard to the tensile strength after 24 hours at room temperture[7].

Stronger types of intrinsic self-healing interactions include metal-ligand interactions and ionic interactions, which typically exhibit a strong temperature-dependency. Dopamine modified poly(ε-caprolactone) showed strong metal-ligand self-healing interactions with Fe_3O_4, recovering 91% of its mechanical properties from a notch test[8]. Poly(urethane) chains terminated with terpyridine were dynamically crosslinked with Zn^{2+} metal ions to introduce self-healing. After being subjected to a heat treatment of 90 °C for 1 hour, the polymer exhibited a 93% recovery of its strain at break[9]. Finally, ionic modification of bromobutyl rubber with butylimidazole introduced dynamic ionic bonds, which enabled the rubber to self-heal. A 90% recovery in the strain at break was observed after self-healing at room temperature for 8 days, and an increase of the temperature to 100 °C increased the rate of self-healing[10].

However, a balance between the mechanical strength of the material and the self-healing ability needs to be achieved. As noted by Suckow et al., the formation of strong ionic clusters within bromobutyl rubber increased tensile strength, but hindered chain mobility and healing significantly[11]. The strength of the ionic clusters was controlled using different length aliphatic chains attached to the rubber. With strong ionic clusters from short aliphatic chains, the self-healing ability of the rubber was reduced severely due to reduced chain dynamics, demonstrating an opposing influence and a ‘tension’ between the need for good mechanical properties and self-healing properties[11].

Grafting of polar groups to polymer backbone can also enhance the polarity of the polymer and increase the relative permittivity, whilst maintaining a low dielectric loss and a high breakdown strength[12-16]. Issues of agglomeration and dispersion that limit the application of extrinsic modification methods can therefore be overcome.

The grafting of allyl cyanide and 3-mercaptopropionitrile have resulted in a relative permittivity increase up to $\varepsilon_r \sim 18$, but the material did not exhibit any self-healing[17, 18]. Allyl cyanide modified silicone elastomers have been used in small scale energy harvester configurations[19].

Of particular interest is the temperature dependencies of the self-healing and electromechanical properties of a polymer, which can be tailored by control of the dynamic chemical interactions. For example, there may be a desire to optimise healing and mechanical properties at room temperature or under more hostile conditions. Non-covalent, electrostatic interactions can break and reform easily at room temperature to introduce a small degree of enhanced self-healing, but can be thermally overcome at higher temperatures[20]. Hydrogen bonding provides the opportunity for a stronger type of intrinsic interaction for self-healing and temperature resistance. To thermally overcome hydrogen bonding, temperatures in excess of 60 °C are typically required to allow the hydrogen bonding groups to break and reform their interactions readily[21]. However, recent research has demonstrated hydrogen bonding initiated self-healing at room temperature. As an example, Chen et al. modified a poly(urethane) with poly(propylene carbonate) to utilise both van der Waals interactions and hydrogen bonding. At 50 °C, the elastomer recovered 100% of its strain at break[22]. However, modification of poly(urethane) with poly(ethylene glycol) and poly(propylene glycol) led to an elastomer with a strain-at-break healing efficiency of 97% at room temperature after 1 day[23, 24].

In this work, we explore a competitive grafting reaction between two different polar groups of methyl thioglycolate (MG) and thioglycolic acid (TG) that was introduced into a commercial elastomer, SBS, via one-pot thiol-ene click-chemistry under ambient conditions. The incorporation of both the electrostatic and hydrogen bonding interactions endowed the MG/TG-SBS hybrid elastomers with properties of interest for dielectric elastomer applications, namely a self-healing function, high strain, high breakdown strength and low loss. By tuning the ratios of the MG/TG groups, the mechanical strength and the hydrogen-bonding network for self-healing and thermal resistance could be tailored whilst retaining the dielectric enhancements in permittivity, which are desirable for energy transduction applications using

dielectric elastomers[16]. New insights on the impact of the hydrogen bonding and electrostatic interactions on the temperature-dependencies of the self-healing and electromechanical properties of the materials were achieved based on a detailed analysis of real-time FTIR, ^{1}H NMR, atomic force microscopy and broadband impedance spectroscopy. This demonstrates the feasibility of tuning self-healing and electromechanical properties of high permittivity, low loss dielectric elastomers by intrinsic chemical modification for actuation and energy harvesting devices at a range of temperature conditions.

2. Experimental

2.1. Materials

Styrene-butadiene-styrene block copolymer (SBS, Vector 8508A) was purchased from Dexco. Tetrahydrofuran (THF, GPR Reactapur, 99.9%) was purchased from VWR, UK. Hexane (for HPLC >95%), chloroform-*d* (99.8%), 2,2-dimethoxy-2-phenylacetophenone (DMPA, 99%), methyl thioglycolate (95%) and thioglycolic acid (99%) were purchased from Sigma-Aldrich, UK.

2.2 Synthesis of MG/TG-SBS

In a typical synthesis of 80/20 MG/TG-SBS, 10 g SBS was dissolved in 90 g of THF. Following this, 0.2 g of DMPA and 4× molar excess of thiol relative to the butadiene block of SBS was added to the solution (37.5 ml of methyl thioglycolate, 7.29 ml of thioglycolic acid). The solution was then irradiated with UV light @ 365 nm with 25% intensity (50 W) using an OmniCure Series 2000 200 W UV lamp for 20 minutes. The resulting modified SBS was purified by precipitation in hexane and dried in a vacuum oven overnight at 60 °C. The mass of the resulting product was 22.0 g (93.4% total grafting, 84.1% methyl thioglycolate grafting and 15.9% thioglycolic acid grafting). ^{1}H NMR (400 MHz, $CDCl_3$): δ = 7.09 (br, 3 H, $H_{benzene}$), 6.55 (br, 2 H, $H_{benzene}$), 3.76 (S, 3 H, COOC**H**$_3$), 3.25 (S, 2 H, OOC-C**H**$_2$-S), 2.77 (br, 1 H, $(CH_2)_2$C**H**S), 2.66 (br, 2 H, H_2CC**H**$_2$S), 1.76 (br, 2 H, H_2C-C**H**$_2$-CH), 1.57 (br, 6 H, (-H_2C)$_2$C**H**$_2$), 1.45 (br, 2 H, -HCC**H**$_2$CH$_2$), 1.28 (br, 1 H, $(H_2C)_3$C**H**) ppm. FT-IR (cm^{-1}): 2929, 1728, 1435, 1273, 1129, 1007, 757.

2.3. Materials characterisation

SBS and MG/TG-SBS were characterised by ^{1}H NMR, all spectra were recorded using a Bruker Avance III HD 400 MHz spectrometer. Chemical shifts were internally referenced to

TMS using $CDCl_3$. Variable temperature ^1H NMR was performed using a Bruker Avance 500 MHz using toluene-d8. Spectra were processed using ACD/NMR processor version 12.01 (ACD/Labs).

Tensile testing was performed using a Shimadzu Autograph AGS-X with samples conforming to ASTM-D638-14 type V. The extension rate was 50 mm min^{-1} (strain rate of 10.95% s^{-1}) with a 10 kN load cell and tests were carried out at room temperature. Stress relaxation was investigated by stretching the specimens to 100% elongation at 50 mm min^{-1} and holding the samples at constant strain for up to 2 hours. Cyclic stress softening was performed by elongating specimens to 100% and 300% elongation and back to 0% under a controlled strain rate of 50 mm min^{-1} for 5 cycles. Self-healing was performed at room temperature or 80 °C and the dogbones were cut using a scalpel and the two exposed faces were pushed back together under finger pressure only. The dogbones were allowed to heal for up to three days at their respective temperature before tensile testing at room temperature.

Fourier transform infrared spectroscopy (FT-IR) was investigated in transmission mode using a Bruker Tensor 27 at a resolution of 4 cm^{-1} with 32 scans ran for the background and the sample. Temperature-dependent FT-IR was performed in transmission mode with an additional Specac Eurotherm 2216e heating stage. UV-Vis was performed using an Agilent Cary 60 photospectrometer between 800 nm and 200 nm. Samples were dissolved in DCM to a concentration of 1×10^{-5} mol dm^{-3}. Dynamic Mechanical Thermal Analysis (DMTA) was performed on samples 10.0 mm × 5.0 mm × 2.3 mm in tensile mode with a 50 μm amplitude and a frequency of 1 Hz and a heating rate of 2 K min^{-1} between -120 °C and 135 °C using a Triton Tritec 2000 DMA. Atomic Force Microscopy (AFM) imaging was done using a Bruker Dimension Icon in Peakforce QNM mode with Scanasyst-Air tips using tapping mode at a scan rate of 0.2 Hz. Impedance spectroscopy measurements were carried out using a Princeton Applied Research Parastat MC with a PMC-2000 card and a two-point probe between 10^0~10^6 Hz on thin films of thickness between 100~200 μm that were formed by compression moulding using a Rondol manual hot press at 190 °C and 5 kN of force over an electrode contact area of 5 cm ×5 cm.

3. Results and Discussion

3.1 Structural characterisation

Tuning the hydrogen bonding group ratio allows the mechanical properties, the self-healing performance and the temperature resistance of the elastomer to be balanced depending on the

properties required for actuator or energy harvesting applications. Both TG and MG groups were grafted to the butadiene block of SBS via a one-pot click-chemistry synthesis, as shown in Figure 1, where the MG/TG-SBS were grafted with MG/TG molar ratios ranging between 100/0 and 80/20, as seen in Figure S1, S2 and S3. The absolute grafting ratio between MG and TG was determined by ^{1}H NMR.

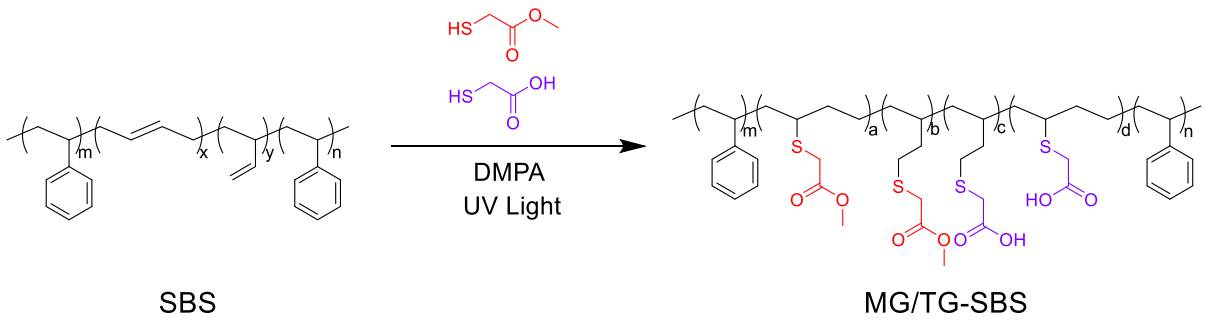

Figure 1 Chemical modification routes of SBS to form MG/TG-SBS. Red compound is methyl thioglycolate, purple compound is thioglycolic acid.

3.2 Synergetic effects of MG/TG on morphology, electromechanical and self-healing properties

3.2.1 Tensile strength and strain to failure

Figure 2a shows the effects of grafting of polar groups on the tensile properties of SBS. Unmodified SBS has a tensile strength of 9 MPa. After grafting with 100/0 MG/TG, the tensile strength was reduced to 3.1 MPa. For mixed grafting of MG/TG groups, the tensile strength of the MG/TG-SBS was 4.40 MPa and 3.31 MPa for 95/5 and 80/20 MG/TG-SBS respectively and was therefore enhanced compared to 100/0 MG/TG-SBS due to the influence of the hydrogen bonding that was introduced by the TG. However, a small decrease in tensile strength to 2.79 MPa is observed for 90/10 MG/TG-SBS, which can be explained by the change in the phase morphology of the polymer and the greater hydrogen-bonding network that was formed; this can be observed in the AFM imaging in Figure 3A.

In terms of the strain to failure, a greater degree of hydrogen bonding yielded a reduction in the strain at break which was decreased to 270% for 80/20 MG/TG-SBS as compared to 100/0 MG/TG-SBS (569%) and pure SBS (857%). Therefore, due to the effect of the hydrogen bonding network on the mechanical properties, it is possible to tune the MG/TG ratio to obtain an optimal strain at break and tensile strength.

3.2.2 Cycle stress softening

The introduction of the dynamic networks into SBS to induce self-healing will affect the interchain interactions and chain mobility, which can be reflected by stress softening behaviour. After five 100% strain cycles during the cyclic stress softening tests, all chemically modified SBS elastomers exhibited a lower hysteresis loss (< 20%) compared to pure SBS (39%), seen in Figure 2b, c and Figure S4. The low hysteresis loss of the modified elastomers is attributed to the electrostatic interaction between the polymer chains producing a change in the morphology and preventing energy loss within the elastomer. After five 300% cycles, the hysteresis loss for 90/10 MG/TG-SBS was 29%, whilst the hysteresis loss for 100/0 MG/TG-SBS and 95/5 MG/TG-SBS remained below 20%. The larger hysteresis loss in 90/10 MG/TG-SBS at higher strain cycles is thought to be a result of the hydrogen-bonding network formed, which is rigid at room temperature. Comparatively, SBS had a hysteresis loss of 58% after five 300% strain cycles.

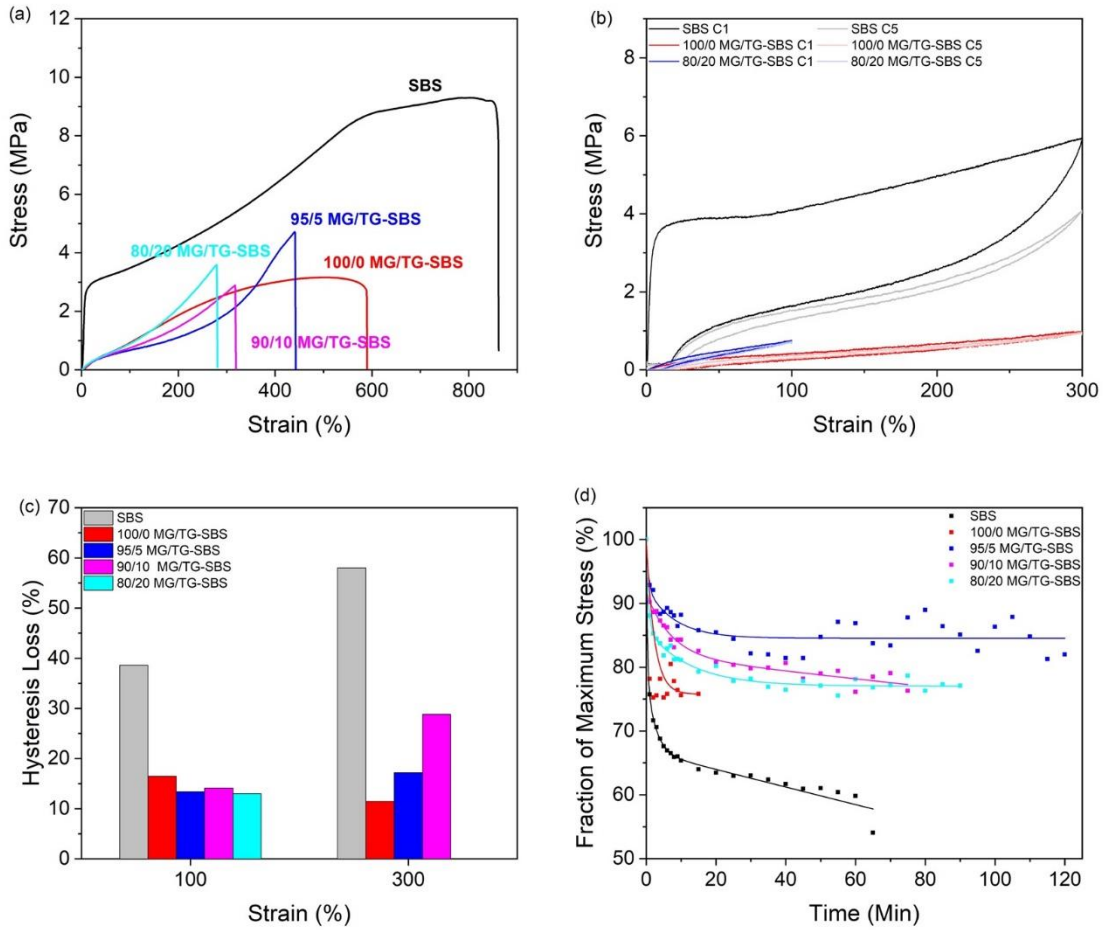

Figure 2 Characterisation of SBS, 100/0, 95/5, 90/10 and 80/20 MG/TG-SBS, (a) Stress-strain curves, (b) First (*C1*) and fifth (*C5*) cycle of cyclic stress softening loops, (c) hysteresis energy loss, and (d) Fraction of maximum stress from stress relaxation over time.

The degree of stress relaxation reflects the change in polymer chain behaviour between SBS and chemically modified SBS. In one hour the stress in SBS fell to 60% of its initial value (σ_{init}), while the stress in the MG/TG-SBS elastomers fell to 75-85% of σ_{init} over the same period, see Figure 2d. In comparison to SBS the stress relaxation is lower in all the MG/TG-SBS elastomers. As will be explained in the sections that follow, this is due to the increased hydrogen bonding and electrostatic interactions as a result of the modifications.

3.2.3 Phase morphology

The enhanced interchain interactions of the modified SBS materials are reflected by the phase morphology transition of SBS. As shown in Figure 3A (a), AFM of unmodified SBS material shows microphase separation morphology, where the cylindrical styrene phase is observed as dark regions surrounded by butadiene regions, shown as a lighter colour; this is also shown in the schematic in Figure 3B. The 95/5 MG/TG-SBS, Figure 3A (b), exhibits a phase morphology with a disordered arrangement of spheres present and the phase structure merges, resulting in a small disordered arrangement of spheres relating to uncompatiblised styrene. The phase separation disappears due to the increased compatibilisation of the two blocks *via* an electrostatic interaction with methyl thioglycolate[20]. Increasing the thioglycolic acid content to 90/10 MG/TG-SBS shows an increase in the number of spheres present, Figure 3A (c), albeit in a disordered fashion. This change in microstructure compared to 100/0 and 95/5 MG/TG-SBS led to a decrease of the tensile strength for 90/10 MG/TG-SBS, shown in Figure 2a. However, the decrease in height distribution in the image (in comparison to the larger height distribution in SBS, see contour maps in Figures 3A (a – c) demonstrates that these new spheres are not a result of phase separation of styrene and butadiene, but are the ordering of thioglycolic acid groups to form a hydrogen bonding network. Finally, increasing the TG grafting further in 80/20 MG/TG-SBS in Figure 3A (d) transforms the phase morphology from a disordered fashion to a regular microstructure arrangement, showing the effect of the hydrogen-bonding network. The progression of phase morphology is also shown schematically in Figure 3B.

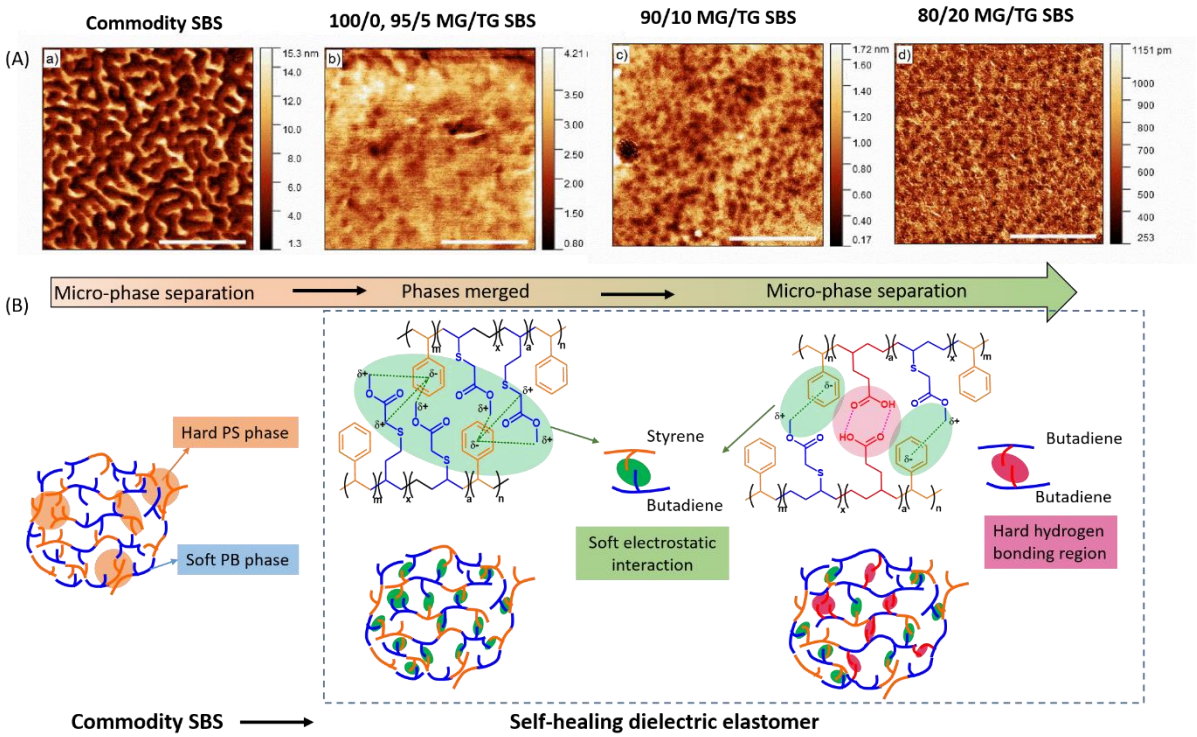

Figure 3 (A) AFM imaging of (a) SBS, (b) 95/5, (c) 90/10 and (d) 80/20 MG/TG-SBS. Scale bars = 200 nm. (B) Schematic to show phase morphology transition corresponding to the AFM images, where the original SBS (30% polystyrene PS) shows phase separation morphology, the grafting of MG group increases the compatibility between PS and polybutadiene (PB) phases due to the electrostatic interactions (green) and results in a single-phase morphology[20]; the additional TG introduces a hydrogen bonding interaction and as the TG content increases, a disorder-to-order phase transition occurs as a result of the phase separation of the hard hydrogen bonding regions (red).

3.2.4 Glass transition temperature (T_g)

The enhanced interchain interaction in the modified SBS is also observed *via* a change in the glass transition temperature (T_g). As indicated in the DMTA data in Figure 4, the original SBS shows two T_g's at -83 °C for butadiene and at 97 °C for styrene. After grafting with 100/0 MG/TG groups, the two peaks merge into a single peak at -22 °C, indicating the compatibilisation of the butadiene and styrene blocks, and the peak has a similar intensity to the poly(butadiene) peak of SBS. Comparatively, the MG/TG-SBS hybrids have a T_g similar to that of 100/0 MG/TG-SBS, but increasing the TG ratio increases T_g up to -18.5 °C. This is because the T_g for purely TG modified SBS is expected to be 20 °C[25]. Additionally, the tan δ

peak intensity increases significantly for all the elastomers, indicating that introduction of hydrogen bonding has reduced the elastic behaviour and increased the energy dissipation within the materials. In 90/10 and 80/20 MG/TG-SBS, a series of small, broad peaks are observed between 40 °C and 100 °C, which are due to the thermal energy inside the system as the hydrogen bonds are free to break and reform as temperature increases and allows polymer chain relaxations. Therefore, the small broad peaks are associated with the hydrogen bonding network formed in the MG/TG-SBS, which supports the atomic force morphology development in Figure 3.

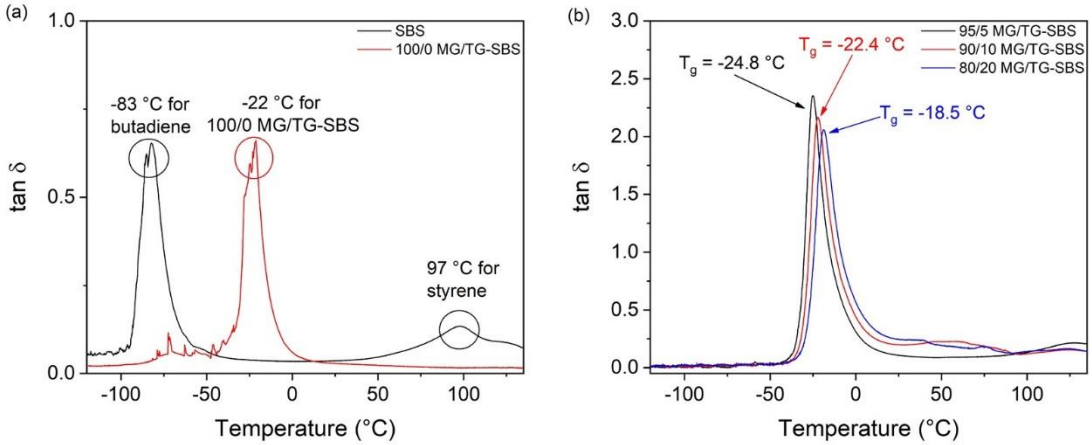

Figure 4 DMTA characterisation of tan δ, (a) SBS and 100/0 MG/TG-SBS and (b) 95/5, 90/10 and 80/20 MG/TG-SBS in the temperature range of -120 to 135 °C

3.2.5 UV-Vis spectroscopy and dielectric properties

UV-Vis spectroscopy in Figure 5 shows the shift in absorption of the aromatic styrene block after chemical modification. The MG/TG-SBS elastomers show that the aromatic peak blue shifts by 15 nm compared to pure SBS, as methyl thioglycolate interacts with the styrene ring. The peak originates from a π-π* transition from styrene rings which are not involved in π-stacking interactions. The blue shift originates from the interaction with δ+ protons either side of the methyl thioglycolate ester interacting with the δ- aromatic centre of styrene, demonstrating that there is an increase in the π-π* transitional energy. As the ratio of polar groups changes in the MG/TG-SBS hybrids, the wavelength of absorption does not shift, demonstrating that the styrene block is still fully interacting with methyl thioglycolate. This demonstrates that the block copolymer type phase morphology observed by AFM in Figure 3 is due to the thioglycolic acid modified regions of the butadiene block rather than phase separation between methyl thioglycolate modified butadiene block and the styrene block.

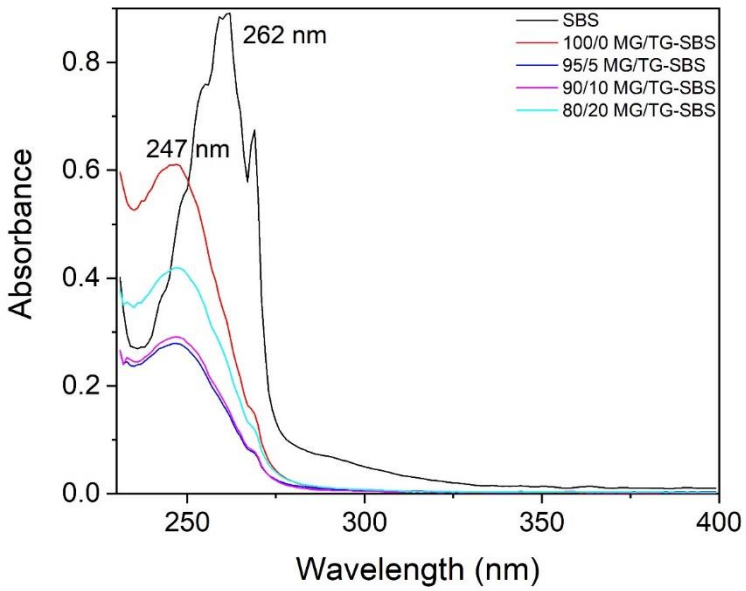

Figure 5: UV-Vis spectroscopy of SBS, 100/0, 95/5, 90/10 and 80/20 MG/TG-SBS

Finally, the effect of the grafting resulted in significantly improved electrical properties compared to SBS. The intrinsic grafting of polar groups led to MG/TG-SBS elastomers exhibiting giant permittivity with an increase from, $\varepsilon_r \approx 2.8$ to $\varepsilon_r \approx 9.2$ at 10^3 Hz after modification. In addition, MG/TG-SBS elastomers were low loss with $\tan \delta \approx 0.01$ at 10^3 Hz for high efficiency energy transduction, similar to that of unmodified SBS (0.009), as seen in Figure S5.

3.3 Temperature-dependency of self-healing and electrical properties

3.3.1 Hydrogen bonding networks

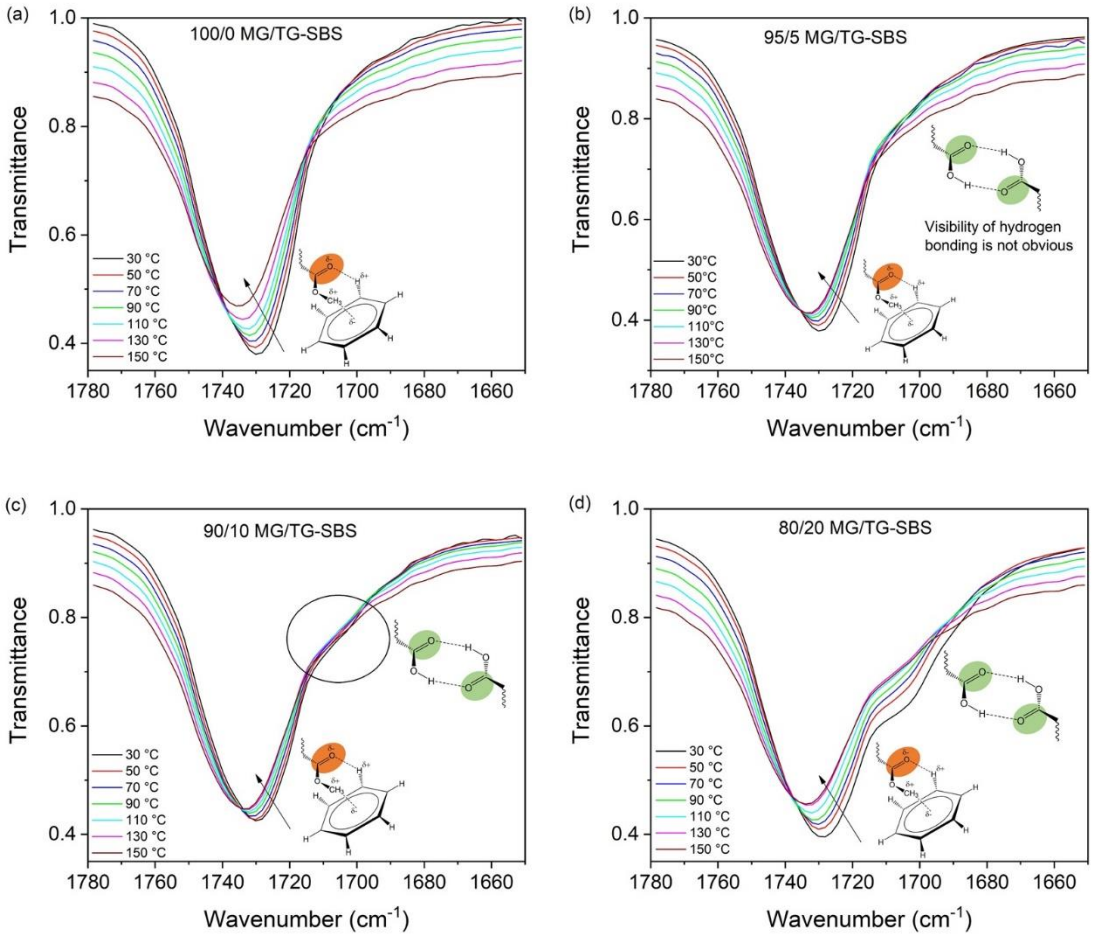

Figure 6 Temperature-dependent FTIR spectrospcopy for MG/TG-SBS at 1730 cm^{-1}: (a) 100/0, (b) 95/5, (c) 90/10 and (d) 80/20.

To understand the differences in the strengths of the hydrogen bonding networks present in MG/TG-SBS elastomers, temperature-dependent FTIR was investigated between 30 °C and 150 °C. This revealed the impact of the reinforcing nature of the hydrogen bonding network and allowed the differences in temperature resistance between the elastomers to be observed, observed in Figure 6 and Figure S9.

Upon heating, the ester C=O absorption peak from methyl thioglycolate increases by 6 cm^{-1} from 1730 cm^{-1} as the temperature is increased from 30 °C to 150 °C in all four elastomers. In 90/10 and 80/20 MG/TG-SBS, the thioglycolic acid hydrogen bonding dimers are observed as a shoulder peak at 1700 cm^{-1} in addition to the methyl thioglycolate ester as the hydrogen-bonding thioglycolic acid content is increased (Figure 6c and d). This is most prominently observed in 80/20 MG/TG-SBS, at 30 °C due to the largest hydrogen-bonding network present. The dimer peak flattens as the temperature is increased. After 90 °C the peak in 80/20 MG/TG-

SBS is no longer visible. However, in 90/10 MG/TG-SBS, the thioglycolic acid dimer peak flattens at 50 °C, showing the reduced temperature resistant nature of the elastomer from a weaker hydrogen bonding network. Additionally, the dimer peak cannot be observed in 95/5 MG/TG-SBS, see Figure 6b.

Furthermore, in Figure S9, a shift of the broad O-H peak is observed in 80/20 MG/TG-SBS upon heating from an approximate centre at 3200 cm^{-1} to 3300 cm^{-1}, as the O-H groups are also freed from the thioglycolic acid dimerization. This change demonstrates that the hydrogen bonding groups now have sufficient thermal energy to break and reform freely, thereby assisting the self-healing process. In 90/10 MG/TG-SBS, the O-H peak is visible until 90 °C, and the loss of this peak indicates a complete loss of the hydrogen bonding network in the elastomer. Finally, the O-H peak is not observed in 95/5 MG/TG-SBS nor in 100/0 MG/TG-SBS.

Overall, the temperature-dependent FTIR peaks provide evidence for the temperature reinforcement effect from the hydrogen bonding network. 80/20 MG/TG-SBS has the greatest reinforcement effect due to the strongest hydrogen bonding network formed. 90/10 MG/TG-SBS demonstrates an improved temperature reinforcement effect, whereas there is no observable difference between 95/5 MG/TG-SBS and 100/0 MG/TG-SBS.

Figure S10 shows variable temperature solution state ^{1}H NMR of 80/20 MG/TG-SBS. At 25 °C, the broad peak of the acid proton, attributed to thioglycolic acid grafted to SBS, is apparent at 8.9 ppm. Increasing the temperature to 50 °C shifts the peak upfield to 8.3 ppm, as the proton environment becomes less deshielded by the rupturing of the hydrogen bonded acid dimer. However, at 50 °C some hydrogen bonding is still present, which is observed as a downfield tailing of the peak[26, 27]. At 70 °C, the downfield tail disappears, indicating that thioglycolic acid is no longer dimerised.

Overall, variable temperature FTIR and ^{1}H NMR demonstrates the strength of the hydrogen bonding present in 80/20 MG/TG-SBS, in good agreement with the schematic in Figure 3B, and the dominance of the network on the polymer structure and behaviour as confirmed by AFM and DMTA.

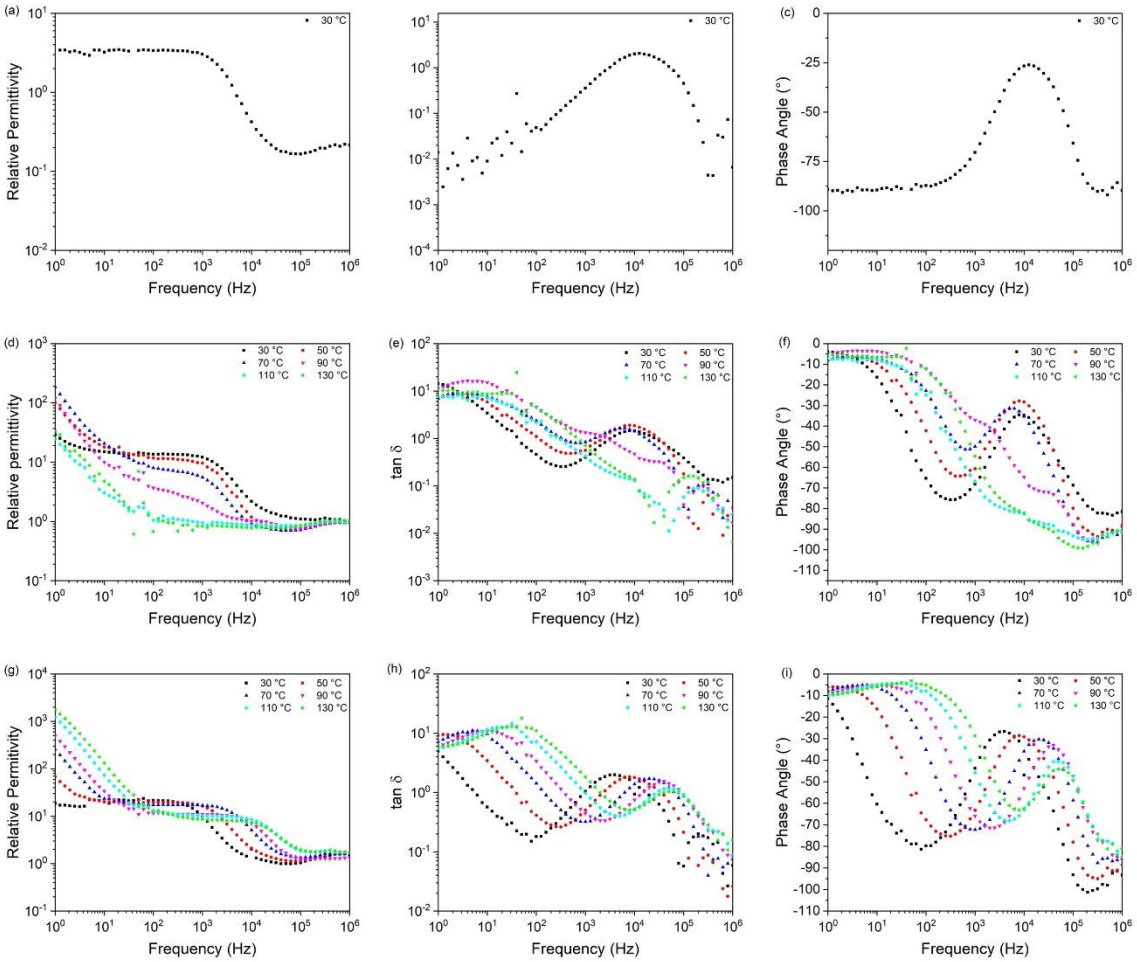

Figure 7 Relative permittivity, tan δ and phase angle of SBS (a-c), 100/0 MG/TG-SBS (d-f) and 80/20 MG/TG-SBS (g-i) between 30 °C and 130 °C

3.3.2 Temperature dependency of dielectric properties

Temperature dependent impedance spectroscopy was used to observe how overcoming the electrostatic interactions and hydrogen bonding interactions through thermal energy affected the electrical properties of 100/0 MG/TG-SBS and 80/20 MG/TG-SBS, Figure 7. SBS has an observable relaxation peak in tan δ and phase angle at 30 °C at 12 kHz, attributed to the frequency at which the polymer chains are no longer able to respond to the applied electric field, as seen in Figure 7 b and c. However, no data could be obtained at 50 °C as SBS had a less solid-like behaviour, reducing the adhesion of the carbon grease electrode.

100/0 MG/TG-SBS exhibited relaxation peaks in tan δ and phase angle up to 90 °C at 9 kHz in Figure 7 e and f. This arises from the polar polymer chains not able to respond to the alternating electric field above this frequency; this is also related to the decrease in relative

permittivity, see Figure 7d. The relaxation peak frequency was lower due to the grafted polar group impeding the response movement of the polymer chains. However, above 90 °C the relaxation peak disappears. This is likely due to the increased thermal energy overcoming the weak electrostatic interaction between methyl thioglycolate and styrene, thus causing the 100/0 MG/TG-SBS dipole to be thermally overcome. Once no dipole is present, no relaxation peak is observed from the polymer chains. Between 30 °C and 70 °C, increases in the relative permittivity and ac conductivity are observed at low frequency (< 100 Hz), as the increased thermal energy increases electron transfer within the polymer structure; this also leads to a phase angle approaching 0° at frequencies below 100 Hz. In this region, electrode polarisation is prevalent. Above 70 °C, the loss of the dipole within 100/0 MG/TG-SBS leads to a reduced conductivity and relative permittivity in this frequency range, as seen in Figure 7 d.

For 80/20 MG/TG-SBS, a relaxation peak is present for all temperatures investigated. The position of the relaxation peak in phase angle and tan δ shifts from 4 kHz at 30 °C to 64 kHz at 130 °C, Figure 7 h and i. The nature of the relaxation peak in 80/20 MG/TG-SBS is attributed to two causes of polarity. Firstly, the same weak electrostatic interaction observed in 100/0 MG/TG-SBS is formed. Secondly, strong hydrogen bonding exists between thioglycolic acid groups. This hydrogen bonding retards the response of the polymer chains to the applied electric field, reducing the frequency of the observed relaxation peak. In addition, the increase in thermal energy on the hydrogen bonding leads to a reduction in the relaxation peak intensity as temperature increases. This is because there is a greater rate of breaking and reforming of hydrogen bonds plus a reduced lifetime of a hydrogen bond. However, the hydrogen bonding is never fully overcome and a dipole remains within 80/20 MG/TG-SBS, thus a relaxation peak is always observed. The relaxation peak shifts to a higher frequency upon increasing the temperature because the increased thermal energy of the polymer chains and the faster breaking/reforming time of the hydrogen bonding allows the polymer chain to respond to the alternating electric field.

At lower frequencies (<100 Hz), 80/20 MG/TG-SBS shows an increase in the relative permittivity and ac conductivity for all temperatures, Figure 7 g. This, once again, is due to the increase in thermal energy promoting the flow of ions, enhancing the electrode polarisation observed.

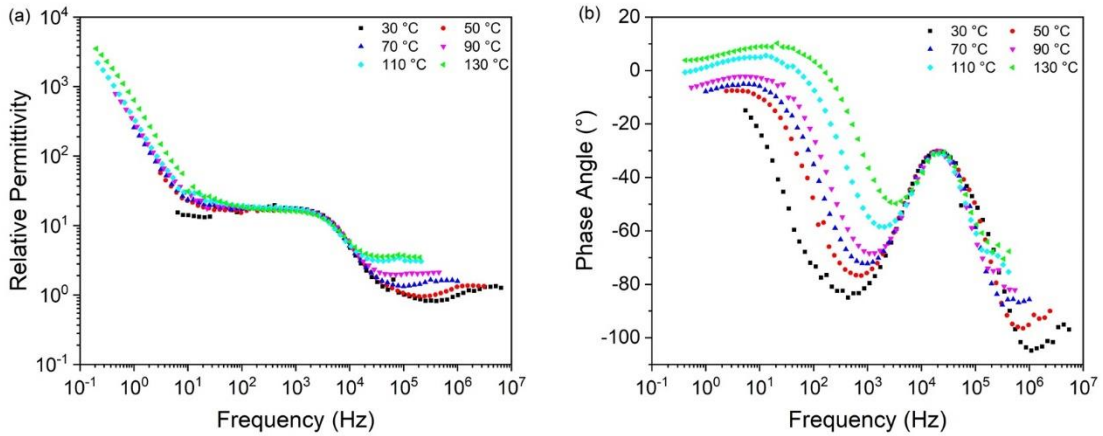

Figure 8 (a) relative permittivity and (b) phase angle master curves for 80/20 MG/TG-SBS for a reference temperature of 70 °C

The experimental data shows that the time-frequency superposition principle[28] can be applied to the relative permittivity and phase angle curves for 80/20 MG/TG-SBS, as shown in Figure 8. The frequency of the curves was shifted by a factor of a(t) using the equation: $a(t) = \frac{t_t}{t_r}$, where t_t is the relaxation time at a specific temperature and t_r is the relaxation time at the reference temperature, 70 °C. Thus the frequency range for 70 °C is extended from 10^{-1} to 10^7 Hz. At low frequencies (<10^2 Hz), electrode polarisation from electrode blocking becomes more prominent in both the relative permittivity and phase angle graphs. A large relaxation peak is observed at 10^4 Hz attributed to the frequency at which the hydrogen bonding thioglycolic acid is no longer able to respond to the electric field. However, no additional structural transitions are observed at higher frequencies (>10^5 Hz) and the relative permittivity remains constant and the phase angle at -90 °, indicating the material is insulating and acting as a capacitor.

3.3.3 Temperature dependency of self-healing properties

The hydrogen-bonding networks present in MG/TG-SBS provide a potential mechanism for temperature dependent self-healing. Investigation into the temperature dependency of self-healing for MG/TG-SBS elastomers was investigated through room temperature and 80 °C self-healing between 100/0 and 80/20 MG/TG-SBS to determine how the strong hydrogen bonding network can influence self-healing.

At room temperature, following three days of self-healing 80/20 MG/TG-SBS exhibited the greatest strain-at-break recovery of 48% corresponding to a strain at break of 139% (Figure 9). At 80 ºC, healing was enhanced significantly. After 3 hours, 80/20 MG/TG-SBS recovered

79% of its strain at break, corresponding to a strain at break of 230%. This synergistic behaviour from the hydrogen bonding network and the electrostatic methyl thioglycolate/aromatic interaction boosted the overall healed strain at break. In fact, the self-healing recovery of all MG/TG-SBS elastomers was greater after 15 minutes at 80 °C than 3 days at room temperature. However, the temperature dependency on the self-healing nature of the elastomers decreases upon reduced thioglycolic acid content, thus the self-healing recovery is less in 95/5 and 90/10 MG/TG-SBS than 80/20 MG/TG-SBS, as seen in Figure S8. Comparatively, 100/0 MG/TG-SBS showed a reduced self-healing ability at 37 °C compared to room temperature self-healing as the increased thermal energy of the polymer chains disrupted the weak electrostatic interaction between methyl thioglycolate and the styrenic blocks – i.e. reducing the compatibilisation and thereby adversely affecting self-healing (Figure 10).

An improvement in the healed tensile strength and tensile strength recovery was observed for all elastomers after 15 minutes in Figure S7-9. Once again, 80/20 MG/TG-SBS exhibited the greatest tensile strength recovery after three hours of 28% (0.93 MPa) due to the greater presence of hydrogen bonding groups. This recovery was significantly higher than healing 80/20 MG/TG-SBS at room temperature for three days (21.4%, 0.71 MPa).

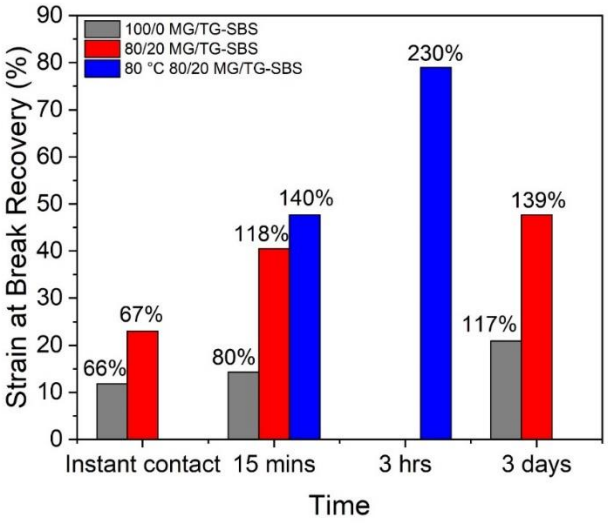

Figure 9 Recovery of strain at break for 80/20 MG/TG-SBS at room temperature and 80/20 MG/TG-SBS at 80 °C for various durations of self-healing. Values for strain at break achieved are shown also. The self-healing properties of 100/0 MG/TG-SBS were included for

comparison. Room temperature self-healing tested after instant contact, 15 mins contact and 3 days contact. 80 °C self-healing tested after 15 minutes and 3 hrs of contact.

With regard to the impact of phase morphology on self-healing, for molecular interdiffusion to take place the fracture surfaces of the polymers must remain in close contact. Such contact will be facilitated by the polymer being soft and by the temperature being well above the glass transition[1, 2, 29, 30]. Continued close contact and growth of the contact area with time, the "wetting" stage, will be assisted by attractive macromolecular interactions. Clearly, the presence of glassy micro-phase in SBS, in this case 30% of hard PS phase as in Figure 3B, impedes the chain interdiffusion and self-healing at the "wetting" stage. The introduction of methyl thioglycolate (MG) groups into the SBS promotes the compatibilization between PS and PB phases due to the electrostatic interactions, as indicated by the AFM (Figure 3A), DMTA (Figure 4) results and schematic in Figure 3B. The material becomes even softer - as seen in the tensile tests, Figure 2, where the 95/5 MG/TG-SBS appears the most rubbery. The further introduction of thioglycolic acid groups (TG) introduces a disorder-to-order phase transition due to the formation of hard hydrogen bonding regions, observed clearly in the AFM and DMTA data and is shown schematically in Figure 3B. The introduction of the MG and TG groups enhances interfacial attraction through both electrostatic and hydrogen bonding interactions, thereby facilitating the "wetting" stage of self-healing.

At room temperature the initial "wetting" stage of self-healing is enhanced by the presence of the hydrogen bonding interaction, while the hydrogen bonding also hinders subsequent polymer chain interdiffusion; therefore Wool & O'Connor theory can be applied to explain that the room-temperature self-healing of 100/0 MG/TG-SBS will overtake that of the 80/20 MG/TG-SBS material over time. In contrast, at 80°C the hydrogen bonding is thermoliable, and no longer presents a significant restraint to the molecular interdiffusion, which leads to a faster self-healing process. The presence of hydrogen bonding interaction also benefits the improved strength of the healed material.

4. Conclusions

New insights on the impact of the hydrogen bonding and electrostatic interactions on the temperature-dependencies of the self-healing and electromechanical properties of chemically modified thermoplastic elastomer SBS materials have been achieved. Mixed polar groups methyl thioglycolate (MG) and thioglycolic acid (TG) were grafted to the alkene groups in the

polymer backbone *via* a one-pot thiol-ene click chemistry. The grafted MG groups allowed enhancement of the intermolecular interactions of SBS, thus providing the materials with self-healing function along with an enhanced relative permittivity, thereby making them well suited to dielectric elastomer applications. The introduction of TG groups further induced hydrogen-bonding among the chains, resulting in enhanced mechanical strength and temperature-resilience of self-healing behaviour of the MG/TG-SBS.

The MG/TG-SBS hybrids achieved a giant relative permittivity of $\varepsilon_r \sim 9.2$ and low losses, and 95/5 MG/TG-SBS material had the largest strain at break at 441.7 %. The strain at break decreased upon increasing the thioglycolic acid content due to the increased hydrogen bonding content. The self-healed 80/20 MG/TG-SBS at 80 °C showed the greatest recovery of its strain at break after 3 hours of 79%, a strain at break of 233%. Furthermore, after just 15 minutes of 80 °C self-healing, the strain at break recovery was already 48%, corresponding with a strain at break of 140%. The degree of hydrogen bonding demonstrated a large influence over the self-healing behaviour of the elastomers, with lower degrees of healing observed upon reduced thiolglycolic acid modification.

Temperature dependent impedance spectroscopy revealed that the weak electrostatic interaction facilitating self-healing in 100/0 MG/TG-SBS is fully overcome at 90 °C, while in 80/20 MG/TG-SBS the relaxation continues to exist at 130 °C. This reinforces the ability to tune the temperature dependent properties exhibited by MG/TG-SBS. Temperature dependent FTIR studies confirms the nature of the self-healing interactions present in MG/TG-SBS elastomers, as there is a large flattening of the C=O peak between 70 °C and 90 °C in 80/20 MG/TG-SBS as the hydrogen bonding is able to break and reform more readily. Due to the high temperature resilience of 80/20 MG/TG-SBS, this elastomer is of interest for actuation and energy harvesting under more hostile conditions.

This work demonstrates that self-healing and electromechanical properties of high permittivity, low loss dielectric elastomers can be controlled by the interactions of polar groups which are also affected by temperature. This detailed analysis provides useful evidence and directions for macromolecular design of high performance dielectric elastomers for sustainable energy transduction applications.

References

1. R. P. Wool and K. M. O'Connor, *J. Appl. Phys.*, 1981, **52**, 5953-5963.
2. R. P. Wool and K. M. O'Connor, *Journal of Polymer Science: Polymer Letters Edition*, 1982, **20**, 7-16.
3. N. I. Khan, S. Halder, S. B. Gunjan and T. Prasad, *IOP Conference Series: Materials Science and Engineering*, 2018, **377**, 012007.
4. Y.-L. Liu and T.-W. Chuo, *Polym. Chem.*, 2013, **4**, 2194-2205.
5. J. Bai, H. Li, Z. Shi, M. Tian and J. Yin, *RSC Adv.*, 2015, **5**, 45376-45383.
6. J.-F. Mei, X.-Y. Jia, J.-C. Lai, Y. Sun, C.-H. Li, J.-H. Wu, Y. Cao, X.-Z. You and Z. Bao, *Macromol. Rapid Commun.*, 2016, **37**, 1667-1675.
7. L. Liu, S. Yan and L. Zhang, *Macromol. Rapid Commun.*, 2018, **39**, 1800349.
8. L. Du, Z.-Y. Xu, C.-J. Fan, G. Xiang, K.-K. Yang and Y.-Z. Wang, *Macromolecules*, 2018, **51**, 705-715.
9. Q. Zheng, Z. Ma and S. Gong, *J. Mater. Chem. A*, 2016, **4**, 3324-3334.
10. A. Das, A. Sallat, F. Böhme, M. Suckow, D. Basu, S. Wießner, K. W. Stöckelhuber, B. Voit and G. Heinrich, *ACS Appl. Mater. Interfaces*, 2015, **7**, 20623-20630.
11. M. Suckow, A. Mordvinkin, M. Roy, N. K. Singha, G. Heinrich, B. Voit, K. Saalwächter and F. Böhme, *Macromolecules*, 2018, **51**, 468-479.
12. J. Lee, H. Kwon, J. Seo, S. Shin, J. H. Koo, C. Pang, S. Son, J. H. Kim, Y. H. Jang, D. E. Kim and T. Lee, *Adv. Mater.*, 2015, **27**, 2433-2439.
13. R. Shankar, T. K. Ghosh and R. J. Spontak, *Adv. Mater.*, 2007, **19**, 2218-2223.
14. M. Amjadi, A. Pichitpajongkit, S. Lee, S. Ryu and I. Park, *ACS Nano*, 2014, **8**, 5154-5163.
15. R. Pelrine, R. Kornbluh, Q. Pei and J. Joseph, *Science*, 2000, **287**, 836-839.
16. C. Ellingford, C. Bowen, T. McNally and C. Wan, *Macromol. Rapid Commun.*, 2018, **39**, 1800340.
17. S. J. Dunki, M. Tress, F. Kremer, S. Y. Ko, F. A. Nuesch, C.-D. Varganici, C. Racles and D. M. Opris, *RSC Adv.*, 2015, **5**, 50054-50062.
18. C. Racles, M. Alexandru, A. Bele, V. E. Musteata, M. Cazacu and D. M. Opris, *RSC Adv.*, 2014, **4**, 37620-37628.
19. C. Racles, M. Ignat, A. Bele, M. Dascalu, D. Lipcinski and M. Cazacu, *Smart Mater. Struct.*, 2016, **25**, 085024.
20. C. Ellingford, R. Zhang, A. M. Wemyss, C. Bowen, T. McNally, u. Figiel and C. Wan, *ACS Appl. Mater. Interfaces*, 2018, DOI: 10.1021/acsami.8b13785.
21. E. Wittenberg, A. Meyer, S. Eggers and V. Abetz, *Soft Matter*, 2018, **14**, 2701-2711.
22. J. Chen, F. Li, Y. Luo, Y. Shi, X. Ma, M. Zhang, D. W. Boukhvalov and Z. Luo, *J. Mater. Chem. A*, 2019, **7**, 15207-15214.
23. Y. Pan, J. Hu, Z. Yang and L. Tan, *ACS Applied Polymer Materials*, 2019, **1**, 425-436.
24. C.-J. Fan, Z.-C. Huang, B. Li, W.-X. Xiao, E. Zheng, K.-K. Yang and Y.-Z. Wang, *Science China Materials*, 2019, **62**, 1188-1198.
25. M. Tian, H. Yan, H. Sun, L. Zhang and N. Ning, *RSC Adv.*, 2016, **6**, 96190-96195.
26. J. G. Morton, C. L. Joe, M. C. Stolla, S. R. Koshland, C. H. Londergan and M. H. Schofield, *J. Chem. Educ.*, 2015, **92**, 1086-1090.
27. S. Grzesiek, F. Cordier and A. J. Dingley, in *Methods Enzymol.*, eds. T. L. James, V. Dötsch and U. Schmitz, Academic Press, 2002, vol. 338, pp. 111-133.
28. C. Hyung Kim and J. Shin, *Bull. Korean Chem. Soc.*, 2002, **23**.
29. Y. H. Kim and R. P. Wool, *Macromolecules*, 1983, **16**, 1115-1120.
30. S. Prager and M. Tirrell, *The Journal of Chemical Physics*, 1981, **75**, 5194-5198.

Acknowledgement

CE thanks EPSRC and Jaguar Land Rover (UK) for funding this PhD studentship.

Additional Information

The authors declare no competing interests

Supporting Information

Figure S1 (a) ^{1}H NMR spectroscopy of SBS, 100/0 MG/TG-SBS and 80/20 MG/TG-SBS and (b) FTIR spectroscopy of SBS, 100/0 MG/TG-SBS and 80/20 MG/TG-SBS

Figure S2 ^{1}H NMR spectroscopy of 95/5, 90/10 and 80/20 MG/TG SBS

Figure S3 FTIR spectroscopy of 95/5, 90/10 and 80/20 MG/TG-SBS

Figure S4 1st and 5th cycles of cyclic stress softening for 95/5, 90/10 and 80/20 MG/TG-SBS

Figure S5 Impedance spectroscopy showing (a) the relative permittivity, (b) tan δ, and (c) phase angle (d) AC conductivity for SBS, 100/0, 95/5, 90/10 and 80/20 MG/TG-SBS vs frequency

Figure S6 Temperature dependant FTIR for 100/0, 95/5, 90/10 and 80/20 MG/TG-SBS at 3320 cm^{-1} upon heating

Figure S7 (a) Healed tensile strength and (b) tensile strength recovery of both room temperature and 80 °C self-healing of 100/0 and 80/20 MG/TG-SBS at different time steps

Figure S8 (a) Healed strain at break and (b) strain at break recovery for 95/5, 90/10 and 80/20 MG/TG-SBS at room temperature and at 80 °C at different time steps

Figure S9 (a) Healed tensile strength and (b) tensile strength recovery of both room temperature and 80 °C self-healing of 95/5, 90/10 and 80/20 MG/TG-SBS at different time steps

Figure S10 Variable temperature ^{1}H NMR of 80/20 MG/TG SBS between 6 and 10 ppm, showing the –OH peak of grafted thioglycolic acid and aromatic region of styrene in SBS in toluene-d8